Temporal evolution of nanoporous layer in off-normally ion irradiated GaSb

D. P. Datta, A. Kanjilal, S. K. Garg, P. K. Sahoo, D. Kanjilal, and T. Som

Citation: Journal of Applied Physics **115**, 123515 (2014); doi: 10.1063/1.4869658
View online: http://dx.doi.org/10.1063/1.4869658
View Table of Contents: http://scitation.aip.org/content/aip/journal/jap/115/12?ver=pdfcov
Published by the AIP Publishing

Temporal evolution of nanoporous layer in off-normally ion irradiated GaSb

D. P. Datta,[1] A. Kanjilal,[2] S. K. Garg,[1] P. K. Sahoo,[3] D. Kanjilal,[4] and T. Som[1,a)]
[1]*SUNAG Laboratory, Institute of Physics, Bhubaneswar 751 005, Odisha, India*
[2]*Department of Physics, School of Natural Sciences, Shiv Nadar University, Gautam Budh Nagar, Uttar Pradesh 203 207, India*
[3]*School of Physical Sciences, National Institute of Science Education and Research, Bhubaneswar 751 005, Odisha, India*
[4]*Inter-University Accelerator Centre, Aruna Asaf Ali Marg, New Delhi 110 067, India*

(Received 7 December 2013; accepted 14 March 2014; published online 27 March 2014)

Room temperature irradiation of GaSb by 60 keV Ar^+-ions at an oblique incidence of 60° leads to simultaneous formation of a nanoporous layer and undulations at the interface with the underlying substrate. Interestingly, with increasing ion fluence, a gradual embedding of the dense nanoporous layer takes place below ridge-like structures (up to the fluence of 1×10^{17} ions cm^{-2}), which get extended to form a continuous layer (at fluences $\geq 4 \times 10^{17}$ ions cm^{-2}). Systematic compositional analyses reveal the co-existence of Ga_2O_3 and Sb_2O_3 in the surface layer. The results are discussed in terms of a competition between ion-induced defect accumulation and re-deposition of sputtered atoms on the surface. © *2014 AIP Publishing LLC*. [http://dx.doi.org/10.1063/1.4869658]

I. INTRODUCTION

Among the III–V semiconductors, GaSb possesses low band gap and high carrier mobility, which make it a semiconductor of choice for high frequency electronic devices and near to mid-infrared optoelectronic devices.[1] In addition, a range of potential applications like near-infrared sub-wavelength laser,[2] tunnel diode,[3] and field effect transistor[4] have stimulated interest on GaSb nanostructures. In parallel to the conventional techniques such as molecular beam epitaxy,[5] metallo-organic chemical vapor deposition,[6] self-catalyzed growth,[7] or electron irradiation,[8] energetic ion irradiation has also been employed to fabricate GaSb nanostructures.[9–13] However, in most of the existing studies,[9–13] ion fluences were limited to $\sim 10^{14}$-10^{16} ions cm^{-2} which led to the formation of cellular nanostructures,[9,10] or nanorods.[11,12] Formation of a porous layer under a smooth top surface has also been shown at low fluences[13] whereas prolonged irradiation results in removal of the top layer—exposing the self-standing structures in vacuum. Development of nanofibers has also been reported for focused ion beam irradiation of GaSb.[14]

In this context, dynamics of GaSb microstructure evolution at higher fluences (up to two orders of magnitude) is yet to be explored, which can have strong implications in terms of other aspects of ion-matter interaction in GaSb. For instance, energetic ion bombardment of semiconductors at higher fluences and oblique incidence angles leads to the formation of self-organized patterns, namely ripples, dots, and facets at various energies.[15–19] In addition, cross-sectional transmission electron microscopy (TEM) studies on obliquely irradiated surface revealed the formation of a periodically modulated amorphous/crystalline (*a*/*c*) interface in parallel to the top surface.[20] Therefore, in the high fluence regime, the interface between the modified layer and the underneath crystalline substrate may play an important role in the evolution of microstructure, especially for obliquely incident medium energy ions.[20] As a matter of fact, in a recent work, Kumar *et al.*[21] have proposed that the pattern formation may be considered to be an interface phenomenon which starts from the *a*/*c* interface and grows towards the surface.

In this article, we show the evolution of a nanoporous layer on a simultaneously formed undulated substrate interface in off-normally Ar^+-ion irradiated GaSb at room temperature (RT) with fluences in the range of 7×10^{16} to 3×10^{18} ions cm^{-2}. In particular, we demonstrate fluence dependent evolution of a nanoporous layer containing fibers. This is followed by a gradual transformation of a ridge-like structure on the outermost surface into a continuous rough surface. The observed evolution of the nanoporous layer is discussed in our qualitative model in light of agglomeration of ion-beam induced vacancies into voids, subsequent void growth under prolonged ion bombardment, and redeposition of sputtered atoms. We also show the coexistence of phases like Ga_2O_3 and Sb_2O_3 using x-ray photoelectron spectroscopy analyses, which corroborates well with our micro-Raman spectroscopic data.

II. EXPERIMENTAL

Irradiation of mirror polished GaSb(100) wafers (sliced into pieces of 1×1 cm^2 area) was carried out at RT using 60 keV Ar^+-ions at an oblique incidence angle of 60° (with respect to the surface normal). The ion fluence was varied from 7×10^{16} to 3×10^{18} cm^{-2} with a constant current density of 5 μA cm^{-2}. Morphological changes of the irradiated samples were investigated by using a field emission scanning electron microscope (Carl-Zeiss) in both plan-view and cross-sectional geometries. The elemental analysis was carried out in plan-view mode by the energy dispersive x-ray spectroscopy (EDS) system (Oxford Instruments), attached to the scanning electron microscope (SEM), using 10 keV electron beam. In addition, surface chemical property was

a)Electronic mail: tsom@iopb.res.in

studied by x-ray photoelectron spectroscopy (XPS) (VG Instruments) using Mg-K_α radiation source ($h\nu = 1254$ eV). Micro-Raman (Renishaw) spectra were also recorded at RT in a backscattering geometry using the 514 nm line of an Ar laser with an average power of ~50 mW on the sample surface.

III. RESULTS AND DISCUSSION

SEM images of ion beam irradiated GaSb substrates are shown in Figs. 1(a)–1(c) (plan-view), and Figs. 1(d)–1(f) (cross-section) for the fluences of 7×10^{16}, 7×10^{17}, and 3×10^{18} ions cm^{-2}, respectively, exhibiting an evolution of extended network of nanoporous structures. Microstructures corresponding to these three specific fluences are presented here as representative ones. The formation of a porous structure is evident in the plan-view mode [Fig. 1(a)] for 7×10^{16} ions cm^{-2}. Here, a network of nanofibers of diameter 15–22 nm can be seen along with ~3 μm long ridge-like structures on top, which are oriented along the direction of the ion beam (depicted by the arrow on the image). However, a very rough irradiated surface containing scattered pores is observed at the fluence of 7×10^{17} ions cm^{-2} [Fig. 1(b)]; the pore density is found to increase further for the maximum fluence of 3×10^{18} ions cm^{-2} [Fig. 1(c)]. In fact, it appears from Figs. 1(a)–1(c) that the ridges extend with increasing fluence to cover the whole irradiated surface.

The cross-sectional SEM (XSEM) images [Figs. 1(d)–1(f)] confirm the formation of a porous layer which gets completely embedded under the topmost rough surface at the highest fluence of 3×10^{18} ions cm^{-2} (discussed above). A random variation in thickness of the porous layer is also evident from Figs. 1(d)–1(f). Taking into consideration both the plan-view and the XSEM images, it becomes clear that the pores observed on the sample surface [see Figs. 1(b) and 1(c)] are voids extended up to the surface. A further close inspection also reveals that the porous layer is built upon an undulating interface of bulk GaSb where small voids are observed all along the interface. These voids are found to be separated from each other by 15–20 nm thick nano-walls and the dimension of voids increases near the top surface [discernible in Fig. 1(d)]. In fact, detail microstructural studies reveal the formation of polycrystalline nanofibers surrounded by amorphous shell-like structures and voids on an undulating GaSb crystalline interface (cross-sectional TEM images not shown here).

Besides Ga and Sb, O has also been detected in all the irradiated samples through EDS measurements. It may be mentioned that interaction of the GaSb substrate with 10 keV electron beam was simulated by using CASINO simulation package.[22] Accordingly, the maximum depth from which x-ray signals can originate was estimated to be 500 nm, comparable to the thickness of the nanoporous layer [as measured from the cross-sectional SEM images shown in Figs. 1(d)–1(f)]. However, due to the porous nature of the structure, the electron beam is expected to penetrate further into the underlying GaSb substrate. Therefore, the EDS signals are effectively collected from the evolved nanoporous layer and a part of the bulk GaSb as well. The fluence dependent change in atomic fractions of O, Ga, and Sb is shown in Fig. 2 (abscissa given in logarithmic scale for a better clarity). In this case, the total atomic fraction of these elements deviates from 100% since C, which is detected in EDS

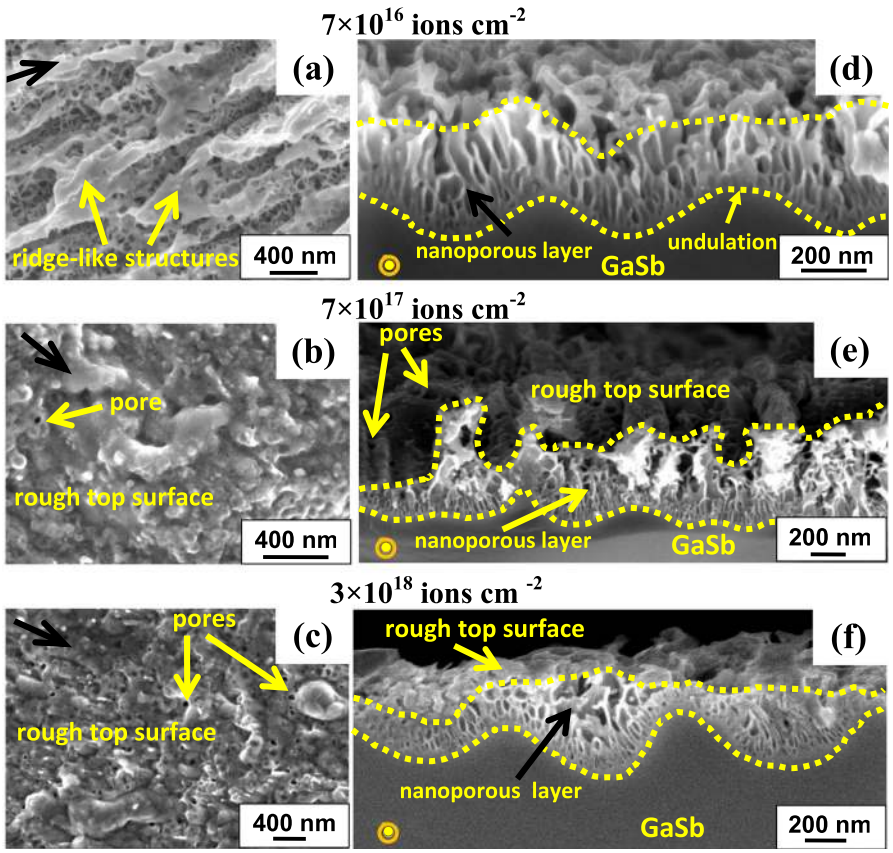

FIG. 1. Plan-view SEM images of GaSb irradiated by 60 keV Ar^+-ions at 60^0 incidence angle to the fluences of (a) 7×10^{16}, (b) 7×10^{17}, and (c) 3×10^{18} ions cm^{-2}. The black arrows in (a), (b), and (c) indicate the projection of ion beam direction onto the surface. Corresponding cross-sectional SEM images are shown in (d), (e), and (f), taken along the direction perpendicular to the projection of the ion beam (beam direction coming out of the page as indicated by concentric yellow circles). The dashed yellow lines on the respective nanoporous layer on the diagrams [(b), (d), and (f)] indicate the top surface and simultaneously formed undulating interface with the underlying GaSb substrate.

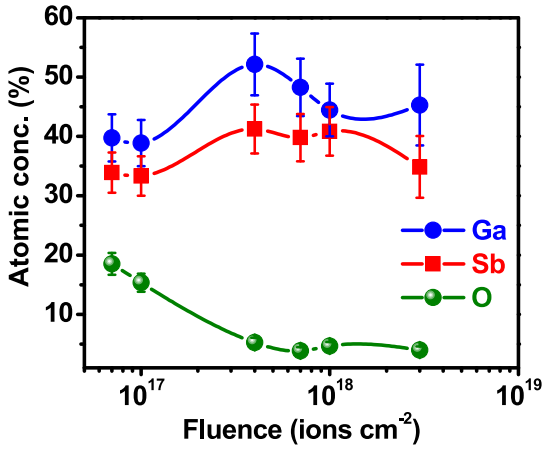

FIG. 2. Atomic concentrations, obtained from EDS analyses, of Ga, Sb, and O as a function of ion fluence. The solid lines are drawn as guides to the eye.

analysis for all the samples, has not been taken into account. As discerned, the atomic concentration of Ga is relatively more compared to Sb for fluences in the range of 7×10^{16} to 4×10^{17} ions cm^{-2}. On the other hand, O concentration decreases gradually up to the same fluence of 4×10^{17} ions cm^{-2}. Interestingly, the continuous top surface starts forming over the nanoporous layer at this fluence itself (not shown). With further increase in the ion fluence, atomic concentrations of Ga and Sb are found to decrease from their maximum values of ~53 and 42 at. % for 4×10^{17} ions cm^{-2} to ~47 and 32 at. %, respectively, for 3×10^{18} ions cm^{-2}, whereas O remains around 5 at. % (Fig. 2).

In order to understand the fluence dependent change in surface chemical properties, we further carried out XPS measurement, where the recorded spectra of the Sb *4d* and the Ga *3d* regions for the pristine and irradiated GaSb samples corresponding to fluences of 7×10^{16}, 7×10^{17}, and 3×10^{18} ions cm^{-2} are shown in Fig. 3. The Sb *4d* core level spectra were deconvoluted into Ga-Sb bonds in GaSb (31.4 eV) and Sb-O bonds in Sb_2O_3 (34.4 eV) with a spin orbit splitting of 1.25 eV.[23] Corresponding Ga *3d* spectra consists of peaks at 19.06 eV, 20.26 eV, and 23.1 eV which are assigned to Ga-Sb bonds in GaSb, Ga-O bonds in Ga_2O_3, and O-Ga bonds due to O *2s* state.[24,25] For the fluence of 7×10^{16} ions cm^{-2}, an additional component in the Sb 4*d* region is found to be located at 31.7 eV, which is attributed to the Sb-Sb bonds of elemental Sb. The additional peak detected in the Ga *3d* spectrum of the pristine sample (at 26 eV) can be assigned to O-C bonds due to surface contamination.[24] Relative amounts of the respective components in the pristine and irradiated samples, as determined from XPS analyses, are summarized in Table I. One can see that the pristine sample surface is highly oxidized (~80%) which is quite common to the GaSb surface.[23,25] While the relative concentration of Ga_2O_3 is found to be increasing by about 10% via removal of C-O bonds with applied fluence, the atomic fraction of Sb_2O_3 is between 40% and 65% (see Table I). An increasing trend of Ga in GaSb phase is observed as a function of fluence, while the presence of elemental Sb is found only for the fluence of 7×10^{16} ions cm^{-2}. As can be seen the relative atomic fraction of Sb in GaSb is larger than that of Ga counterpart throughout the fluence range. This in turn indicates that Ga is more reactive to O, which will be discussed below. The concentration ratio of Sb and Ga in the pristine and irradiated samples has been determined by using the formula,

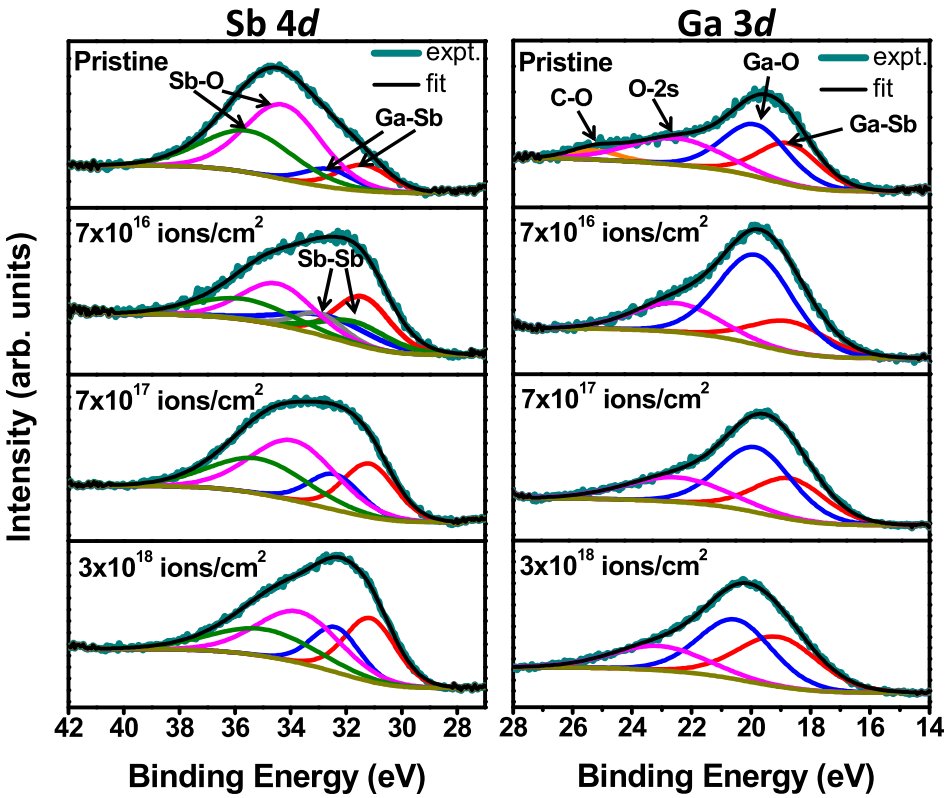

FIG. 3. Ga 3*d* and Sb 4*d* XPS spectra corresponding to pristine and irradiated GaSb samples to the fluences of 7×10^{16}, 7×10^{17}, and 3×10^{18} ions cm^{-2}. The corresponding microstructures are shown in Fig. 1.

TABLE I. Composition of pristine and irradiated GaSb surfaces as extracted from XPS. The relative concentration of different components of Ga and O was determined by analyzing the Ga 3*d* peak, while the relative concentration of different components of Sb was extracted by analyzing the Sb 4*d* peak. The concentration ratio of Sb/Ga is determined by analyzing the Ga 3*d* and Sb 4*d* peaks together.

Sb/Ga	Ga in GaSb	Ga in Ga_2O_3	O in O-C	Sb-Sb	Sb in GaSb	Sb in Sb_2O_3	Sb/Ga
B.E. (eV) / Fluence (ions cm^{-2})	19.06	20.26	26	31.7/32.95	31.4/32.65	34.27/35.52	
0	8.9	79.0	12.1	…	19.2	80.8	0.90
7×10^{16}	8.2	91.8	…	21.3	38	40.7	0.42
7×10^{17}	10.7	89.3	…	…	35.5	64.5	0.51
3×10^{18}	15.3	84.7	…	…	43.6	56.4	0.50

$$\frac{n_{Sb}}{n_{Ga}} = \frac{A_{Sb}/S_{Sb}}{A_{Ga}/S_{Ga}}, \quad (1)$$

where A is the area under the curve, S is the atomic sensitivity factor of the respective elements, viz., Sb and Ga.[26] Using the S values of Ga 3*d* and Sb 4*d* obtained from Ref. 26, the calculated Sb/Ga ratio at different fluences was calculated and is presented in Table I. The Sb/Ga ratio is found to be 0.9 in the pristine sample. For the sample irradiated to the fluence of 7×10^{16} ions cm^{-2} (with exposed nanoporous layer), Sb/Ga ratio reduces to 0.42 which indicates much higher surface concentration of Ga compared to Sb. On the other hand, an increase in the Sb/Ga ratio is noticed at higher fluences (e.g., 7×10^{17} and 3×10^{18} ions cm^{-2}), where a continuous top surface is formed above the porous layer.

To substantiate the XPS results, micro-Raman studies were performed on GaSb samples before and after Ar-ion irradiation. Raman spectra collected from the pristine and the samples irradiated to the fluences of 7×10^{16}, 7×10^{17}, and 3×10^{18} ions cm^{-2} are shown in Fig. 4. Ion bombardment is seen to diminish the clearly visible peak appearing at 236 cm^{-1} corresponding to the LO mode of crystalline GaSb.[27,28] The origin of the peak at 224 cm^{-1} which appears for all irradiated samples is twofold. At the first instance it can be assigned to the TO mode of GaSb which becomes stronger with ion beam irradiation.[27] It can be mentioned that albeit the TO mode in (100) oriented GaSb is forbidden, it gets activated for ion beam irradiation induced highly damaged surface nanoporous layer.[27] Second, considering the forbidden TO mode in GaSb(100) surface, the observed red shift of the LO mode from 236 cm^{-1} (pristine) to 224 cm^{-1} (after irradiation) can be explained in light of phonon confinement effect in the oxidized nanofibers.[14] The strong peak at 144 cm^{-1} is recorded for 7×10^{16} ions cm^{-2}, which can be attributed to the A_{1g} mode of Sb as previously demonstrated for ion beam irradiated GaSb.[14,27,28] Upon deconvoluting the Raman spectra, the presence of additional peaks becomes obvious (as seen from Fig. 4). The peaks at 157 and 167 cm^{-1} match well with Ga_2O_3 (Refs. 29 and 30) whereas the one at 185 cm^{-1} has a close proximity with Sb_2O_3.[31] On the other hand, the broad peak at 256 cm^{-1} (corresponding to 7×10^{16} ions cm^{-2}) can be assigned to Sb_2O_3.[31] Thus, the micro-Raman study corroborates the XPS results well.

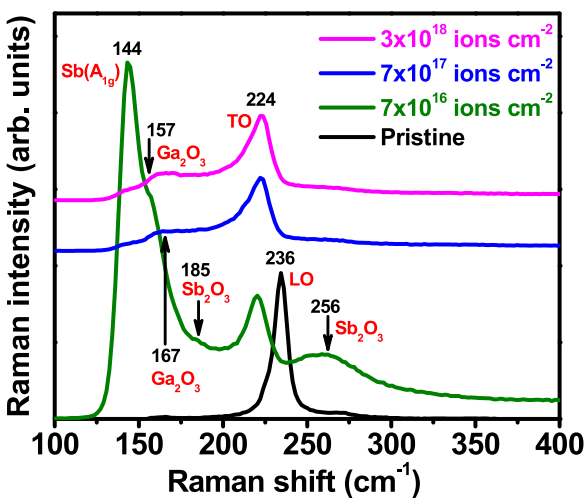

FIG. 4. Micro-Raman spectra of pristine and irradiated GaSb to the fluences of 7×10^{16}, 7×10^{17}, and 3×10^{18} ions cm^{-2}. The spectra are shifted along the ordinate for a better projection.

In order to understand the observed microstructural evolution, we put forward a qualitative framework which is presented in the form of schematic diagrams shown in Figs. 5(a)–5(d). Figure 5(a) shows ion path (dashed blue arrows) and projected ion range in the GaSb bulk substrate. Ion-irradiation induced porosity development in GaSb is presently understood in terms of irradiation induced increase in vacancy concentration along the ion path and subsequent coalescence of vacancies into voids.[9–13] The increase in vacancy concentration originates from highly inefficient recombination of Frenkel pairs because the mobile interstitials precipitate into extended defects like dislocation loops and microtwins.[11,32] Voids grow with further irradiation due to the migration of more ion-generated vacancies. Once a void containing layer is formed as indicated by the dotted black line in Fig. 5(b), incident ions loose energy only within the regions separating the voids while no energy loss occurs for ion paths through the voids. This leads to higher penetration depth of ions into the GaSb substrate than the projected ion range [shown in Fig. 5(a)], as schematically illustrated for two ion paths at positions "1" and "2" in Fig. 5(b). Higher ion penetration results in nucleation of new voids

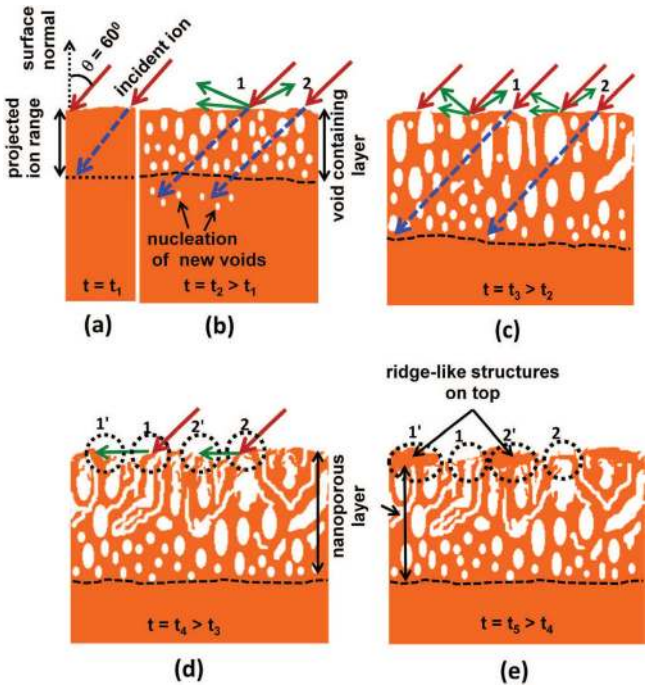

FIG. 5. Schematic representation of the processes resulting in the formation of an embedded nanoporous layer in GaSb with irradiation time, "*t*." Here the dashed blue arrows represent the ion path inside GaSb. The green arrows depict atoms sputtered from the surface. The dotted black line on the diagrams (b)–(e) denotes interface of nanoporous layer and the underlying GaSb substrate.

below the existing void containing layer [see Fig. 5(b)], thus increasing the layer thickness, while the existing voids grow in size with occasional formation of smaller voids in between them. As ion irradiation progresses, this process leads to a final thickness of the void containing layer much larger compared to the projected ion range [depicted in Fig. 5(c)] so that the porous/bulk GaSb interface is located at a depth up to which the incident ions reach after dissipating the energy through the same [represented by the tip of the arrows at positions "1" and "2" in Fig. 5(c)]. At the same time, due to increase in dimension and number density of voids under prolonged ion bombardment, the thin regions between the voids finally result in a network of GaSb nanofibers, as schematically shown in Fig. 5(d). This qualitative model is further supported by recent simulation studies on ion irradiation induced structural evolution of a material,[33] where a fibrous layer is seen to yield from voids.

To understand the formation of a rough top surface on the nanoporous layer within our qualitative model, we consider sputtering and redeposition of sputtered atoms on the growing nanoporous surface which were not considered in either of the earlier models[9,10,13] albeit they are important especially in case of medium energy irradiation in the high fluence regime (as in the present experiment). From the TRIDYN[34] simulation of sputtering yield $Y(\theta)$, as a function of ion incidence angle θ, we find that the total sputtering yield of Ga and Sb under 60 keV Ar^+-ion irradiation of GaSb at 60° is almost three times higher than the same at normal (0°) incidence. Following Refs. 35 and 36, a fraction of atoms sputtered from a region of surface [e.g., positions "1" and "2" in Fig. 5(d)] at large angles from the average surface normal (i.e., at grazing angles to the surface) can be expected to get redeposited on those parts of the growing nanoporous surface, which face the point of ejection [regions "1′" and "2′" in Fig. 5(d)]. In case of oblique ion incidence, in addition to the larger sputtering yield, the number of atoms ejected in the direction of projection of the ion beam on the surface [along the green arrows in Fig. 5(d)] is expected to be larger compared to other directions. It is observed that for normal ion incidence, in the same fluence range, the SEM images (not shown) indicate that a continuous top surface layer does not form on the nanoporous layer. Therefore, obliquely incident ion irradiation induced enhanced redeposition of sputtered particles on top of the growing nanoporous surface seems to be the reason behind the observed formation of ridge-like structures at lower fluences [schematically represented in position "1′" and "2′" in Fig. 5(e)]. Here the parallel orientation of the ridges with the ion beam is due to selective sputtering along the ion beam direction. As the ion bombardment progresses, extension of the ridge-like structures due to prolonged redeposition can result in the formation of a continuous top surface. Thus, in our qualitative model, the embedding of nanoporous layer at high fluences turns out to be the outcome of the simultaneously operative void growth driven nanofiber formation with sputtering and redeposition on the top surface. To further explore the validity of this mechanism, we estimated the angular distribution of sputtered atoms with respect to the surface normal during 60 keV argon irradiation of GaSb by TRIDYN simulation. The number of atoms sputtered at an angle greater than 80° (which is considered, as an example, the lower limit of emission angle for atoms to be redeposited onto the surface) turns out to be three times higher for 60° than that at 0°, which supports our qualitative understanding of transition from ridge-like to continuous surface due to enhanced redeposition at oblique ion incidence.

Although a nanoporous layer of uniform thickness has been observed earlier,[13] to the best of our knowledge, there exists no report on the formation of such a layer extending from an undulating bulk GaSb under ion irradiation at oblique incidence. Formation of periodic surface undulations like ripples or dots on semiconductors under energetic ion bombardment (from hundreds of eV to tens of keV) is well-known[15–21,37,38] and are interpreted due to an interplay between sputtering induced surface-roughening and surface-smoothening processes such as surface diffusion. Medium energy ion induced simultaneous formation of undulating *a*/*c* interface in parallel to the surface has also been reported previously[20,21] where the energy of the incident ions is expected to be very low near the undulating interface. Unlike medium energy ion induced ripple formation in Si, as described above, the absence of any undulated top surface above the nanoporous layer and the presence of only an undulated interface (without any periodicity) with the underneath substrate below the same, in GaSb, at the same energy is remarkable. In addition, a continuous amorphous layer was seen to form in Si[20,21] between these parallel modulations. It may also be mentioned that an open top surface accompanied by an underlying undulated amorphous interface was

observed in case of porous Ge (and swelling) evolving under MeV ion-irradiation although this aspect was not addressed theoretically.[39] However, porosity in irradiated Ge developed after amorphization,[40–42] which is not the case for GaSb where the nanoporous layer is not an amorphous one as discussed above. In fact, in the present case, the nanoporous layer evolves on an undulating interface with ridge-like structures on top in the early stage of irradiation (fluences: 7×10^{16}-1×10^{17} ions cm^{-2}), which after prolonged irradiation (fluences: $\geq 4 \times 10^{17}$ ions cm^{-2}) transform into a continuous rough top surface. In other words, modulated interface (with the underlying substrate) in GaSb is formed before the formation of the top surface under irradiation and therefore, they seem to be uncorrelated with each other.

Let us now try to understand the observed surface morphology in light of ion erosion, which in the past was considered to be responsible for evolution of periodic surface topography.[15–21,37,38] In case of GaSb, preferential sputtering during low energy ion irradiation was considered to be an important factor leading to Ga enrichment at the surface and associated morphological evolution.[37,38,43–46] However, TRIDYN simulation for 60 keV Ar-ion irradiation of GaSb provides sputtering yields of Ga (Y_{Ga}) and Sb (Y_{Sb}) which are very close to each other. Thus, it may be inferred that albeit preferential sputtering will contribute in the present case, it alone would be insufficient to explain the observed evolution of surface morphology accompanied by a Ga-rich surface. In addition, analyses of the irradiated surfaces reveal that the surface composition deviates significantly from the stoichiometric GaSb, which makes it even difficult to estimate exact sputtering yields. As a whole, complete understanding of the morphological evolution of the top surface with such dynamically evolving compositional changes still remains far from clear.

Regarding the modulated interface, it may be noted that upon using very low ion energies (100–1800 eV), dimension of the reported periodic surface modulations in GaSb is in the range of 15–80 nm,[16,37,38] which is an order of magnitude less than those (400–800 nm) seen in the present case (Fig. 1). Thus, formation of the observed undulated interface is difficult to be explained only by considering very low ion energies available near the underlying substrate and remains an open problem.

The oxidation of the ion-exposed samples, as realized from the XPS data, can be attributed to the exposure of the irradiated sample surfaces to air[47] as the native oxide layer on the pristine GaSb should get sputtered out at high fluences used in the present experiment. The higher oxidation of Ga compared to Sb (Table I) is also consistent with the respective Gibbs free energies[48] of Ga_2O_3 (−238.6 kcal/mol) and Sb_2O_3 (−151.5 kcal/mol), which makes Ga_2O_3 more stable. In addition, the oxidized Sb may further react with GaSb in the following manner: $Sb_2O_3 + 2GaSb \rightarrow Ga_2O_3 + 4Sb$.[12] However, the final composition of the oxidized surface is limited by kinetic and diffusional barriers and may contain both the oxides instead of the thermodynamic instability of Sb_2O_3.[49] The presence of elemental Sb in the nanoporous layer, observed from XPS and Raman data, at the lowest fluence of 7×10^{16} ions cm^{-2} is also consistent with the above argument and agrees well with the results of Kluth *et al.*[12] Elemental Sb is also detected corresponding to the fluence of 1×10^{17} ions cm^{-2} where nanofibers get partially exposed (in between the ridge-like structures) to vacuum. When a rough top surface is formed at a higher fluence ($>1 \times 10^{17}$ ions cm^{-2}), XPS probes the top surface where relatively lower oxidation might take place due to a reduction in the exposed surface area compared to the nanoporous layer in early stage of irradiation (Fig. 2). In fact, the absence of elemental Sb at higher fluences (see Fig. 4 and Table I) indicates the presence of Sb only in the nanofibers. Thus, the observed enhancement in Sb/Ga ratio, determined from the XPS data (Table I), can be attributed to irradiation as well as oxidation induced Ga segregation. Similar oxidation induced Ga segregation, leading to Ga-rich surface, has been observed in low energy ion-irradiation of GaSb as well.[43–46]

Due to the formation of exposed nanoporous structure at the fluence of 7×10^{16} ions cm^{-2}, effective surface area is higher than the smooth surface of the pristine sample. When the continuous surface layer is formed at higher fluences, a reduction in the exposed surface area is possibly the reason for a small decrease in the Ga concentration. EDS analyses also indicate a similar increase in Ga in the intermediate fluence range and a reduction at higher fluences. However, the quantitative analysis based on EDS data deviates from the XPS results because EDS probes much higher depth of the irradiated samples (~500 nm) compared to XPS.

IV. CONCLUSIONS

In summary, we have shown the impact of 60 keV Ar^+-ions on GaSb(100) wafers at RT under oblique incidence (60°) in the hitherto unexplored high fluence regime, and demonstrated the formation of a nanoporous layer on a simultaneously formed undulating interface with the underlying GaSb substrate. This is accompanied by the formation of ridge-like structures atop the nanoporous layer at lower fluences ($\leq 1 \times 10^{17}$ ions cm^{-2}) whereas a continuous but rough top surface evolves at higher fluences ($\geq 4 \times 10^{17}$ ions cm^{-2}). Results are explained in terms of a qualitative model where formation of the continuous top surface is attributed to the redeposition of sputtered atoms from the nanoporous layer at its top under obliquely incident ion bombardment. In addition, XPS analyses show that the nanofibers get oxidized—containing Ga_2O_3 and Sb_2O_3 phases which are further corroborated by micro-Raman measurements. The observed oxidation of the nanofibers would be useful for their potential applications in catalytic devices or as gas sensors.[50,51] More experiments at different ion incidence angles, energies, fluences, and temperatures are underway to have better control over the observed micro-structural changes and gather more physical insights on the processes leading to such changes.

ACKNOWLEDGMENTS

Authors gratefully acknowledge helps received from Professor Shikha Varma, Institute of Physics, Bhubaneswar for XPS studies, and Pravakar Mallick, National Institute of

Science Education and Research, Bhubaneswar for SEM measurements. Authors would also like to acknowledge helps from Sriparna Chatterjee, Institute of Minerals and Materials Technology, Bhubaneswar along with Tanmoy Basu and Mohit Kumar, SUNAG Laboratory, Institute of Physics for their helps during this study.

[1]P. S. Dutta, H. L. Bhat, and V. Kumar, J. Appl. Phys. **81**, 5821 (1997).
[2]A. H. Chin, S. Vaddiraju, A. V. Maslov, C. Z. Ning, M. K. Sunkara, and M. Meyyappan, Appl. Phys. Lett. **88**, 163115 (2006).
[3]B. M. Borg, M. Ek, B. Ganjipour, A. W. Dey, K. A. Dick, L.-E. Wernersson, and C. Thelander, Appl. Phys. Lett. **101**, 043508 (2012).
[4]B. M. Borg, K. A. Dick, B. Ganjipour, M. E. Pistol, L. E. Wernersson, and C. Thelander, Nano Lett. **10**, 4080 (2010).
[5]M. Ahmad Kamarudin, M. Hayne, R. J. Young, Q. D. Zhuang, T. Ben, and S. I. Molina, Phys. Rev. B **83**, 115311 (2011).
[6]Y. N. Guo, J. Zou, M. Paladugu, H. Wang, Q. Gao, H. H. Tan, and C. Jagadish, Appl. Phys. Lett. **89**, 231917 (2006).
[7]S. Schulz, M. Schwartz, A. Kuczkowski, and W. Assenmacher, J. Cryst. Growth **312**, 1475 (2010).
[8]H. Yasuda, A. Tanaka, K. Matsumoto, N. Nitta, and H. Mori, Phys. Rev. Lett. **100**, 105506 (2008).
[9]N. Nitta, M. Taniwaki, Y. Hayashi, and T. Yoshiie, J. Appl. Phys. **92**, 1799 (2002).
[10]N. Nitta and M. Taniwaki, Physica B: Condens. Matter **376–377**, 872 (2006).
[11]S. M. Kluth, J. D. Fitz Gerald, and M. C. Ridgway, Appl. Phys. Lett. **86**, 131920 (2005).
[12]P. Kluth, S. M. Kluth, B. Johannessen, C. J. Glover, G. J. Foran, and M. C. Ridgway, J. Appl. Phys. **110**, 113528 (2011).
[13]A. Perez-Bergquist, S. Zhu, K. Sun, X. Xiang, Y. Zhang, and L. Wang, Small **4**, 1119 (2008).
[14]X. Zhou, W. Guo, A. G. Perez-Bergquist, Q. Wei, Y. Chen, K. Sun, and L. Wang, Nanoscale Res. Lett. **6**, 6 (2011).
[15]C. S. Madi, E. Anzenberg, K. F. Ludwig, Jr., and M. J. Aziz, Phys. Rev. Lett. **106**, 066101 (2011).
[16]T. Allmers, M. Donath, and G. Rangelov, J. Vac. Sci. Technol. B **24**, 582 (2006).
[17]D. P. Datta and T. K. Chini, Phys. Rev. B **69**, 235313 (2004).
[18]J. R. Mohanty, T. Basu, D. Kanjilal, and T. Som, Appl. Surf. Sci. **258**, 4139 (2012); T. Som, T. K. Chini, Y. S. Katharia, S. Tripathy, and D. Kanjilal, Appl. Surf. Sci. **256**, 562 (2009).
[19]T. Basu, D. P. Datta, and T. Som, Nanoscale Res. Lett. **8**, 289 (2013).
[20]T. K. Chini, F. Okuyama, M. Tanemura, and K. Nordlund, Phys. Rev B **67**, 205403 (2003).
[21]T. Kumar, A. Kumar, and D. Kanjilal, Appl. Phys. Lett. **103**, 131604 (2013).
[22]P. Hovington, D. Drouin, and R. Gauvin, Scanning **19**, 1 (1997).
[23]Z. Y. Liu, T. F. Kuech, and D. A. Saulys, Appl. Phys. Lett. **83**, 2587 (2003).
[24]I. Geppert, M. Eizenberg, A. Ali, and S. Datta, Appl. Phys. Lett. **97**, 162109 (2010).
[25]V. M. Bermudez, J. Appl. Phys. **114**, 024903 (2013).
[26]C. D. Wagner, L. E. Davis, M. V. Zeller, J. A. Taylor, R. H. Raymond, and L. H. Gale, Surf. Interface Analysis **3**, 211 (1981).
[27]S. G. Kim, H. Asahi, M. Seta, J. Takijawa, S. Emura, R. K. Soni, and S. Gonda, J. Appl. Phys. **74**, 579 (1993).
[28]J. H. Dias da Silva, S. W. da Silva, and J. W. Galzerani, J. Appl. Phys. **77**, 4044 (1995).
[29]Y. H. Gao, Y. Bando, T. Sato, Y. F. Zhang, and X. Q. Gao, Appl. Phys. Lett **81**, 2267 (2002).
[30]J. Li, X. Chen, Z. Qiao, M. He, and H. Li, J. Phys.: Condens. Matter **13**, L937 (2001).
[31]B. S. Naidu, M. Pandey, V. Sudarsan, R. K. Vatsa, and R. Tewari, Chem. Phys. Lett **474**, 180 (2009).
[32]R. Callec and A. Poudoulec, J. Appl. Phys. **73**, 4831 (1993).
[33]K.-D. Li, A. Perez-Bergquist, and L. Wang, Nucl. Instrum. Methods. Phys. Res. B **267**, 3063 (2009).
[34]W. Möller, W. Eckstein, and J. Biersack, Comp. Phys. Commun. **51**, 355 (1988).
[35]J. Belson and I. H. Wilson, Nucl. Instrum. Methods Phys. Res. B **182–183**, 275 (1981).
[36]M. Zier and W. Hauffe, Nucl. Instrum. Methods Phys. Res. B **202**, 182 (2003).
[37]S. Facsko, T. Dekorsy, C. Koerdt, C. Trappe, H. Kurz, A. Vogt, and H. L. Hartnagel, Science **285**, 1551 (1999).
[38]S. Facsko, T. Bobek, H. Kurtz, T. Dekorsy, S. Kyrsta, and R. Cremer, Appl. Phys. Lett. **80**, 130 (2002).
[39]B. Stritzker, R. G. Elliman, and J. Zou, Nucl. Instrum. Methods Phys. Res. B **175–177**, 193 (2001).
[40]L. M. Wang and R. C. Birtcher, Appl. Phys. Lett. **55**, 2494 (1989).
[41]L. M. Wang and R. C. Birtcher, Philos. Mag. A **64**, 1209 (1991).
[42]M. C. Ridgeway *et al*., Phys. Rev. Lett. **110**, 245502 (2013).
[43]W. Yu, J. L. Sullivan, and S. O. Saied, Surf. Sci. **352–354**, 781 (1996).
[44]S. Le Roy, E. Barthel, N. Brun, A. Leragre, and E. Søndergård, J. Appl. Phys. **106**, 094308 (2009).
[45]O. El-Atwani, J. P. Allain, and A. Suslova, Appl. Phys. Lett. **101**, 251606 (2012).
[46]O. El-Atwani, S. Gondeman, and J. P. Allain, J. Appl. Phys. **114**, 104308 (2013).
[47]R. Callec, P. N. Favennec, M. Salvi, H. L'Haridon, and M. Gauneau, Appl. Phys. Lett. **59**, 1872 (1991).
[48]S. Mcdonnel, D. M. Zhernokletov, A. P. Kirk, J. Kim, and R. M. Wallace, Appl. Surf. Sci. **257**, 8747 (2011).
[49]Z. Y. Liu, B. Hawkins, and T. F. Kuech, J. Vac. Sci. Technol. B **21**, 71 (2003).
[50]K. Nakagawa, M. Okamura, N. Ikenaga, T. Suzuki, and T. Kobayashi, Chem. Commun. **1998**(9), 1025.
[51]L. Mazeina, V. M. Bermudez, F. K. Perkins, S. P. Arnold, and S. M. Prokes, Sens. Actuators B: Chem. **151**, 114 (2010).